

Spin Controlled Coexistence of 0 and π States in $SFSFS$ Josephson Junctions

Mohammad Alidoust^{1,*} and Klaus Halterman^{2,†}

¹*Department of Physics, Faculty of Sciences, University of Isfahan, Hezar Jerib Avenue, Isfahan 81746-73441, Iran*

²*Michelson Lab, Physics Division, Naval Air Warfare Center, China Lake, California 93555, USA*

(Dated: October 28, 2018)

Using the Keldysh-Usadel formalism, we theoretically study the $0-\pi$ transition profiles and current-phase relations of magnetic $SFSFS$ and $SFSFFS$ Josephson nanojunctions in the diffusive regime. By allowing the magnetizations of the ferromagnetic layers to take arbitrary orientations, the strength and direction of the charge supercurrent flowing through the ferromagnetic regions can be controlled via the magnetization rotation in one of the ferromagnetic layers. Depending on the junction parameters, we find opposite current flow in the ferromagnetic layers, revealing that remarkably such configurations possess well-controlled $0-$ and $\pi-$ states simultaneously, creating a three-terminal $0-\pi$ spin switch. We demonstrate that the spin-controlled $0-\pi$ profiles trace back to the proximity induced odd-frequency superconducting correlations generated by the ferromagnetic layers. It is also shown that the spin-switching effect can be more pronounced in $SFSFFS$ structures. The current-phase relations reveal the important role of the middle S electrode, where the spin controlled supercurrent depends crucially on its thickness and phase differences with the outer S terminals.

PACS numbers: 74.50.+r, 74.45.+c, 74.25.Ha, 74.78.Na

I. INTRODUCTION

It has been over a decade since hybrid structures of ferromagnets and superconductors began to attract considerable interest from a fundamental physics perspective as well as from the viewpoint of practical devices.¹⁻⁶ The singlet Cooper pair amplitudes oscillate and simultaneously decay in the vicinity of the ferromagnet (F)-superconductor (S) interface.^{7,8} This decaying oscillatory behavior leads to interesting and intriguing phenomena such as $0-\pi$ transitions which can take place by varying the system temperature, Thouless energy, exchange field, degree of magnetization inhomogeneity, or inelastic impurities.^{2,9-12,14,51,61} These π -junctions have shown promise as building blocks for quantum computing,¹⁵ thus resulting in extensive studies of these systems in the clean, diffusive, and nonequilibrium regimes.^{31,34,36-40,46,54,57,58}

In a uniform F layer that is proximity coupled to a singlet superconductor, the pair wavefunction is composed of an odd-frequency triplet component in addition to the usual even-frequency singlet component.^{11,16,41,42} The only triplet correlations that can exist in this case are those with zero total spin projection $m = 0$ on the spin quantization axis. Both the singlet superconducting correlations and this type of odd-frequency triplet correlations oscillate and sharply decay inside the F layer.^{1,11,16,59} However, if the magnetization of an F layer possesses an inhomogeneous texture, another triplet component can arise which has non-zero ($m = \pm 1$) spin projection along the spin quantization axis.^{1,11,45,48,50,52} These triplet correlations are shown to penetrate deep into a diffusive F medium with a penetration length the same as conventional singlet correlations in a normal metal.^{42,47}

The existence of such triplet correlations have also been observed in experiments, including the measurement of a triplet supercurrent flowing through Holmium hybrid structures.^{24-27,47} Shortly thereafter, theoretical works explained these findings²⁵⁻²⁷ in terms of spin triplet proximity effects, extending previous studies involving inhomogeneous magnetization patterns^{28,47}. Triplet correlations can

also be generated in half-metallic systems due to spin-active interfaces.^{31,49,50,58,60} Recently it has been predicted theoretically that these types of triplet correlations can arise in ballistic bilayers of ferromagnets with different thicknesses attached to s -wave superconductors.^{33,53,55,56} Such spin superconducting correlations are therefore of interest because they might play important an important role in dissipationless spintronic devices.^{1,2,6,53}

Recently, a new class of Josephson junctions have been experimentally realized in systems consisting of an IsF section (I : insulator layer, sF : a stacked layer that shows superconducting (s) and ferromagnetic properties) sandwiched between two S terminals.¹⁷⁻²⁰ It was shown that the system can operate as a series of SIs and sFS junctions whose properties can be controlled by the thickness of middle s layer. This type of system was also recently studied theoretically,²³ and two operating modes were found depending on the critical thickness of the s layer, equal to $\pi\xi_S/2$, where ξ_S is the superconducting coherence length. Also motivated by the experiments above, a theoretical work investigated the tunability of the magnetic moment due to the triplet correlations by varying the superconducting phase difference of the outer S banks in *symmetric* layered $SFSFS$, and $SFFSFFS$ structures.²¹

If the superconductivity in the middle S layer of a $SFSFS$ nanojunction is not externally controlled, a self-consistent approach²² is needed to properly determine the magnitude and phase of the superconducting pair correlations²³. This situation can be realized by constructing a stack of three layers (FsF) where the middle s layer exhibits superconducting properties below a critical temperature while the other layers are insensitive to temperature. Therefore, by sandwiching the FsF sample between two S banks and cooling the system temperature below the critical temperature, proximity induced modifications arise in the central layer.¹⁷⁻²⁰ This class of configurations and approach used is in contrast to a setup where the macroscopic phase in the middle S layer is assumed to be controlled externally.²¹ Three-terminal Josephson junctions have been experimentally realized in the search

for Majorana Fermions,⁶⁸ in Superconductor/Semiconductor heterostructures.^{69–72} In this work, we also assume that supercurrents are generated via three external superconducting terminals. This is clarified in Fig. 1, where we illustrate our setup for F layers that are sandwiched between the superconducting leads. We moreover assume that the system has *no symmetry* in configuration space along the x -axis, thus requiring full numerical methods to precisely determine the supercurrent transport characteristics.

We consider both $SF SFS$ and $SF SFFS$ type junctions in the diffusive regime. We demonstrate that the transport of supercurrent in each F region can be easily controlled by the relative magnetization orientation of one of the F layers. We show that this valve effect follows in part from the triplet components involved in supercurrent transport arising from the superconducting phase gradients present among the S terminals. Throughout our calculations we have assumed that the macroscopic phase of the three superconducting terminals can be externally varied, and hence the charge current is not necessarily conserved within the S regions. In the F regions, the charge current is constant, but the spin-current is in general not conserved due to the exchange interaction. We employ the Keldysh-Usadel quasiclassical method in the diffusive limit to study these multilayer systems. We then decompose the total supercurrent into both its even- and odd-frequency components, and investigate their spatial profiles as a function of various values of magnetization orientations and phase differences. We demonstrate that the total charge supercurrent in one F can change sign by means of magnetization rotation in one of the other F layers, while the total charge supercurrent does not undergo a reversal in the rotated F layers (or vice versa). This behavior of the current indicates that it is possible to arrange a sequence of controllable 0 and π Josephson junctions in a three terminal $SF SFS$ spin switch. By studying the current components as a function of position, we are able to pinpoint the origin of the spin-controlled supercurrent. Typically in the middle S region, the singlet contribution to the supercurrent follows a nearly linear spatial variation, while the nonvanishing odd-frequency triplet components do not decay in space.

We are able to extract from our numerical results analytical expressions for the current-phase relations, thus simplifying the overall physical picture. The numerical solutions showed that all components of the supercurrent are described by a simple sinusoidal relation that depends on the differences of the phases, θ_L, θ_R , and θ_M , corresponding to the left, right, and middle S regions respectively (see Fig. 1). We found that an additional term arises in the current-phase relations besides the regular sinusoidal terms, which for sufficiently thick middle S electrodes is responsible for spin-controlled transport through the junction. Although this additional term is present for all d_S , its signatures are more prominent when quasiparticle tunneling between outer S electrodes is suppressed, corresponding to the regime of large d_S . Therefore, depending on the superconducting phase differences involving θ_L, θ_R , and θ_M , a relatively thick middle S electrode can limit the spin-controlled features described above.

The paper is organized as follows. In Sec. II we discuss

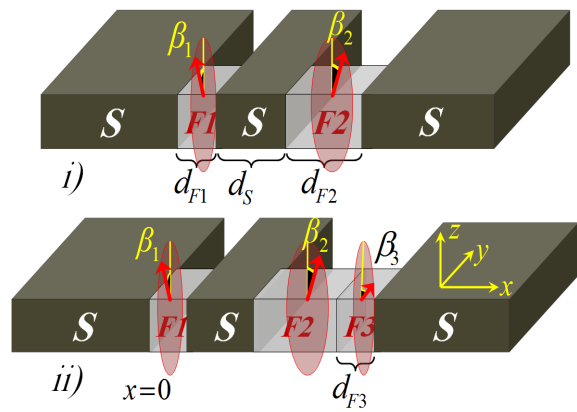


FIG. 1. (Color online) Schematic of the two types of Josephson junctions considered: *i)* $SF SFS$ and *ii)* $SF SFFS$. We assume the SF interfaces are located in the zy plane while the x axis is along the direction of Josephson current flow. The length of the middle superconductor S and ferromagnets F are d_S , d_{F1} , d_{F2} , and d_{F3} , respectively. Throughout the paper, we denote the ferromagnetic regions by F_1 , F_2 , and F_3 as labeled. The exchange field of the magnetic layers is assumed to have arbitrary orientation, $\vec{h} = (h_x, h_y, h_z) = h_0(\cos \gamma \sin \beta, \sin \gamma \sin \beta, \cos \beta)$, in which h_0 is the amplitude of the exchange field. To analyze the system properties without loss of generality, all magnetizations are considered to reside in the zy plane where $\gamma = 0$, and consequently the magnetization orientations can be described solely by β . We therefore define $\beta_{1,2,3}$ for each magnetic layer.

the method employed, details of our assumptions, and technical points used in our calculations. In Sec. III we discuss our results, analyze them and suggest possible applications of our findings. We finally summarize and give the concluding remarks in Sec. IV.

II. THEORY AND METHODS

In this section, we outline the assumptions present and the theoretical approach used to study $SF SFS$ and $SF SFFS$ type systems. The Keldysh-Usadel technique employs the total Green's function with three blocks labeled Retarded (R), Advanced (A), and Keldysh (K). Using the labeled blocks, the total Green's function is represented by¹¹;

$$\hat{G}(\vec{r}, \varepsilon, T) = \begin{pmatrix} G^A & G^K \\ \mathbf{0} & G^R \end{pmatrix}, \quad G^R = \begin{pmatrix} g^R & f^R \\ -\tilde{f}^R & -\tilde{g}^R \end{pmatrix}. \quad (1)$$

The propagators are position, \vec{r} , and temperature, T , dependent. The quasiparticles' energy is denoted by ε and is measured from Fermi level. In the equilibrium steady state, the advanced and Keldysh blocks can be related via $G^A = -(\hat{\rho}_3 G^R \hat{\rho}_3)^\dagger$ and $G^K = \tanh(\beta\varepsilon)(G^R - G^A)$ in which $\hat{\rho}_3$ is the third component of Pauli matrices $\vec{\hat{\rho}} = (\hat{\rho}_1, \hat{\rho}_2, \hat{\rho}_3)$ (see Appendix) and $\beta = k_B T/2$, with k_B the Boltzmann constant. In the absence of a ferromagnetic exchange field, the total Green's function reduces to a 4×4 propagator.^{1,11} However, in the presence of a general exchange field term, the total

Green's function becomes a 8×8 matrix.²⁵ In the regime in which proximity effects are small, we may expand the Green's function around the bulk solution¹¹ $\hat{G}_0 = \text{diag}(1, -1)$, i.e. $\hat{G} \approx \hat{G}_0 + \hat{f}$. In this approximation we arrive at,^{29,30,52}

$$\hat{G}^A = \begin{pmatrix} -1 & 0 & -f_{\uparrow\uparrow}^R(-\varepsilon) & f_{-}^R(-\varepsilon) \\ 0 & -1 & f_{+}^R(-\varepsilon) & -f_{\downarrow\downarrow}^R(-\varepsilon) \\ [f_{\uparrow\uparrow}^R(\varepsilon)]^* & -[f_{-}^R(\varepsilon)]^* & 1 & 0 \\ -[f_{+}^R(\varepsilon)]^* & [f_{\downarrow\downarrow}^R(\varepsilon)]^* & 0 & 1 \end{pmatrix}, \quad (2)$$

in which the asterisk denotes complex conjugation. The arrays with $\uparrow\uparrow$, and $\downarrow\downarrow$ correspond to the spin-one (equal-spin) components while those with \pm represent the superconducting correlations with zero spin (opposite-spin pairing).^{52,63}

The general form of Usadel equation⁴⁴ (which can be derived from the Eilenberger equation⁴³) in the presence of an exchange field with components $\vec{h} = (h_x, h_y, h_z)$ in the ferromagnetic layers, and a gap energy Δ associated with the s -wave superconducting region, can be compactly expressed by⁶²,

$$D[\hat{\partial}, \hat{G}[\hat{\partial}, \hat{G}]] + i[\varepsilon\hat{\rho}_3 - \hat{\Delta} + \text{diag}[\vec{h} \cdot \vec{\tau}, (\vec{h} \cdot \vec{\tau})^T], \hat{G}] = 0, \quad (3)$$

where T denotes transpose, $\hat{\rho}_3$ and $\vec{\tau}$ are 4×4 and 2×2 Pauli matrices, respectively. The matrices are defined in the Nambu and spin spaces which are given in Appendix. Here D is diffusive constant of the highly impure medium and the brackets imply commutator algebra.⁶² The gradient operator is written shorthand as $\hat{\partial}$, such that $\hat{\partial} = (\partial_x, \partial_y, \partial_z)$, which for our one dimensional system reduces simply to ∂_x . Here $\hat{\Delta}$ is a 4×4 matrix that is defined as follows:⁶²

$$\hat{\Delta} = \begin{pmatrix} 0 & 0 & 0 & \Delta \\ 0 & 0 & -\Delta & 0 \\ 0 & \Delta^* & 0 & 0 \\ -\Delta^* & 0 & 0 & 0 \end{pmatrix}. \quad (4)$$

In the ferromagnet regions, the superconducting gap energy Δ in Eq. (3), should be equal to zero while in the diffusive nonmagnetic superconducting layers, the exchange energy \vec{h}

is set equal to zero. The proximity effect that governs the interaction between the differing media is accounted for by the appropriate boundary conditions at the junctions and interfaces. To accurately model realistic barrier regions, we use Kupriyanov-Lukichev boundary conditions at both SF interfaces near the end of the sample;³⁵

$$\zeta(\hat{G}\hat{\partial}\hat{G}) \cdot \vec{n} = [\hat{G}_{\text{BCS}}(\theta_{L,R}), \hat{G}], \quad (5)$$

where \vec{n} is a unit vector normal to the interface. The leakage of correlations are governed by the parameter ζ , which depends on the resistance of the interface and the diffusive normal region.^{6,29,30} The bulk solution, $\hat{G}_{\text{BCS}}(\theta_{L,R})$, for an s -wave superconductor is;⁶²

$$\hat{G}_{\text{BCS}}^R(\theta_{L,R}) = \begin{bmatrix} \mathbf{1} \cosh(\vartheta_{L,R}(\varepsilon)) & i\tau_2 \sinh(\vartheta_{L,R}(\varepsilon)) e^{i\theta_{L,R}} \\ i\tau_2 \sinh(\vartheta_{L,R}(\varepsilon)) e^{-i\theta_{L,R}} & -\mathbf{1} \cosh(\vartheta_{L,R}(\varepsilon)) \end{bmatrix} \quad (6)$$

$$\vartheta_{L,R}(\varepsilon) = \text{arctanh}\left(\frac{|\Delta_{L,R}|}{\varepsilon}\right).$$

We write $\Delta_{L,R}$ for the superconducting gap in the leftmost (L) and rightmost (R) bulk superconductors. On the other hand, we assume that the other interfaces are fully transparent (no insulating layer) for both composite SFS Josephson junction configurations.

The Usadel equation in the general form given above, involving the magnetic exchange field with arbitrary orientation, leads to 8 coupled complex partial differential equations, even in the low proximity limit where the equations can be linearized. It should be reiterated in passing that the interaction between inhomogeneous ferromagnets and s -wave superconductors leads to triplet correlations with nonzero projection along the spin quantization axis.¹¹ Therefore, we may assume that the Green's function describing such systems can be considered as a summation of singlet (\mathbb{S}) and triplet ($\vec{\mathbb{T}}$) components (spin parameterization).^{11,52} We thus write^{52,63}:

$$\hat{f}(\varepsilon) = i(\mathbb{S}(\varepsilon) + \vec{\mathbb{T}}(\varepsilon) \cdot \vec{\tau}) \tau_y, \quad (7)$$

where $\vec{\tau} = (\tau_x, \tau_y, \tau_z)$ is a vector comprised of Pauli matrices. If we now substitute this decomposition of the anomalous Green's function into the Usadel equation Eq. (3), we end up with the following coupled set of differential equations:

$$D \{ \mp \partial_x^2 \mathbb{T}_x(-\varepsilon) + i \partial_x^2 \mathbb{T}_y(-\varepsilon) \} + i \{ -2\varepsilon(\mp \mathbb{T}_x(-\varepsilon) + i \mathbb{T}_y(-\varepsilon)) \mp 2\mathbb{S}(-\varepsilon)(h_x \mp i h_y) \} = 0, \quad (8)$$

$$D \{ \mp \partial_x^2 \mathbb{S}(-\varepsilon) + \partial_x^2 \mathbb{T}_z(-\varepsilon) \} + i \{ \mp 2\mathbb{T}_x(-\varepsilon) h_x \mp 2\mathbb{T}_y(-\varepsilon) h_y - 2(\mp \mathbb{S}(-\varepsilon) + \mathbb{T}_z(-\varepsilon))(\varepsilon \pm h_z) \} = \pm 2i \Delta_M e^{i\theta_M}, \quad (9)$$

$$D \{ \mp \partial_x^2 \mathbb{T}_x^*(\varepsilon) - i \partial_x^2 \mathbb{T}_y^*(\varepsilon) \} + i \{ \pm 2(h_x \pm i h_y) \mathbb{S}^*(\varepsilon) - 2\varepsilon(\mp \mathbb{T}_x^*(\varepsilon) - i \mathbb{T}_y^*(\varepsilon)) \} = 0, \quad (10)$$

$$D \{ \mp \partial_x^2 \mathbb{S}^*(\varepsilon) + \partial_x^2 \mathbb{T}_z^*(\varepsilon) \} + i \{ 2(-\varepsilon \pm h_z)(\mp \mathbb{S}^*(\varepsilon) + \mathbb{T}_z^*(\varepsilon)) \pm 2h_x \mathbb{T}_x^*(\varepsilon) \pm 2h_y \mathbb{T}_y^*(\varepsilon) \} = \mp 2i \Delta_M e^{-i\theta_M}. \quad (11)$$

Since we need to solve the Usadel equations in the central S layer, we denote the superconducting gap in this region by Δ_M , with macroscopic phase θ_M . If the decomposition in Eq. (7) is substituted into the Kupriyanov-Lukichev boundary

conditions (Eq. (5)), the following differential equations must

be satisfied at the left SF interface:³⁰

$$(\zeta\partial_x - c^*(\varepsilon))(\mp\mathbb{T}_x(-\varepsilon) + i\mathbb{T}_y(-\varepsilon)) = 0, \quad (12)$$

$$(\zeta\partial_x - c^*(\varepsilon))(\mp\mathbb{S}(-\varepsilon) + \mathbb{T}_z(-\varepsilon)) = \mp s^*(\varepsilon), \quad (13)$$

$$(\zeta\partial_x - c^*(\varepsilon))(\mp\mathbb{T}_x^*(\varepsilon) - i\mathbb{T}_y^*(\varepsilon)) = 0, \quad (14)$$

$$(\zeta\partial_x - c^*(\varepsilon))(\mp\mathbb{S}^*(\varepsilon) + \mathbb{T}_z^*(\varepsilon)) = \pm s^*(\varepsilon). \quad (15)$$

Here we define the following expressions for $s(\varepsilon)$ and $c(\varepsilon)$,^{10,11,62}

$$s(\varepsilon) = \frac{-\Delta \text{sgn}(\varepsilon)\Theta(\varepsilon^2 - \Delta^2)}{\sqrt{\varepsilon^2 - \Delta^2}} + \frac{i\Delta\Theta(\Delta^2 - \varepsilon^2)}{\sqrt{\Delta^2 - \varepsilon^2}}, \quad (16)$$

$$c(\varepsilon) = \frac{|\varepsilon| \Theta(\varepsilon^2 - \Delta^2)}{\sqrt{\varepsilon^2 - \Delta^2}} - \frac{i\varepsilon\Theta(\Delta^2 - \varepsilon^2)}{\sqrt{\Delta^2 - \varepsilon^2}}, \quad (17)$$

in which $\Theta(x)$ represents a step-function. Likewise, performing the same decomposition for the right FS interface and assuming that both outer superconducting terminals have equal superconducting gaps $\Delta_L = \Delta_R = \Delta$, the Kupriyanov-Lukichev boundary conditions become:³⁰

$$(\zeta\partial_x + c^*(\varepsilon))(\mp\mathbb{T}_x(-\varepsilon) + i\mathbb{T}_y(-\varepsilon)) = 0, \quad (18)$$

$$(\zeta\partial_x + c^*(\varepsilon))(\mp\mathbb{S}(-\varepsilon) + \mathbb{T}_z(-\varepsilon)) = \pm s^*(\varepsilon), \quad (19)$$

$$(\zeta\partial_x + c^*(\varepsilon))(\mp\mathbb{T}_x^*(\varepsilon) - i\mathbb{T}_y^*(\varepsilon)) = 0, \quad (20)$$

$$(\zeta\partial_x + c^*(\varepsilon))(\mp\mathbb{S}^*(\varepsilon) + \mathbb{T}_z^*(\varepsilon)) = \mp s^*(\varepsilon). \quad (21)$$

To investigate the system, the transformed coupled differential equations and associated boundary conditions must be solved using geometrical and material parameters that are experimentally appropriate. Unfortunately, this complicated system of coupled differential equations can be simplified and decoupled for only a limited range of parameters and configurations. When such simplifications are possible, the equations have the advantage that sometimes they can lead to analytical results. However, for our complicated multilayer configurations, numerical methods are the most efficient and sometimes the only possible routes to investigate the relevant transport properties.

One of the most important physical quantities related to transport is the supercurrent that is generated from the macroscopic phase differences between superconducting terminals separated by a ferromagnet. To determine the charge supercurrent, we consider the general expression for the charge current density in the steady state. This involves the Keldysh component of total Green's function via,^{11,62,63}

$$J_x(x) = J_0 \int d\varepsilon \text{Tr}\{\hat{\rho}_3(\hat{G}[\hat{\partial}, \hat{G}])^K\}. \quad (22)$$

Here J_0 is a normalization constant equal to $eN_0D/8$ in which e is the electron charge and N_0 is the density of states of a normal metal at the Fermi surface. To derive a tractable expression for the charge supercurrent density, the Advanced and Keldysh blocks of the Green's function are obtained from the previously mentioned relations above that relate the A , R , and K blocks stemming from Eq. (7). We assume that the current is flowing along the x axis, normal to the interfaces located in the yz plane (see Fig. 1). After some lengthy calculations, we

arrive at the current density:

$$J(x) = J_0 \int_{-\infty}^{\infty} d\varepsilon \{ \mathbb{S}(\varepsilon)\partial_x\mathbb{S}^*(-\varepsilon) - \mathbb{S}(-\varepsilon)\partial_x\mathbb{S}^*(\varepsilon) + \mathbb{S}(\varepsilon)^*\partial_x\mathbb{S}(-\varepsilon) - \mathbb{S}(-\varepsilon)^*\partial_x\mathbb{S}(\varepsilon) - \partial_x\mathbb{T}_x(-\varepsilon)\mathbb{T}_x^*(\varepsilon) + \partial_x\mathbb{T}_x(\varepsilon)\mathbb{T}_x^*(-\varepsilon) - \partial_x\mathbb{T}_x^*(-\varepsilon)\mathbb{T}_x(\varepsilon) + \partial_x\mathbb{T}_x^*(\varepsilon)\mathbb{T}_x(-\varepsilon) - \partial_x\mathbb{T}_y(-\varepsilon)\mathbb{T}_y^*(\varepsilon) + \partial_x\mathbb{T}_y(\varepsilon)\mathbb{T}_y^*(-\varepsilon) - \partial_x\mathbb{T}_y^*(-\varepsilon)\mathbb{T}_y(\varepsilon) + \partial_x\mathbb{T}_y^*(\varepsilon)\mathbb{T}_y(-\varepsilon) - \partial_x\mathbb{T}_z(-\varepsilon)\mathbb{T}_z^*(\varepsilon) + \partial_x\mathbb{T}_z(\varepsilon)\mathbb{T}_z^*(-\varepsilon) - \partial_x\mathbb{T}_z^*(-\varepsilon)\mathbb{T}_z(\varepsilon) + \partial_x\mathbb{T}_z^*(\varepsilon)\mathbb{T}_z(-\varepsilon) \} \tanh(\varepsilon\beta/2). \quad (23)$$

As can be seen, the integration covers the entire quasiparticle energy spectrum. To obtain the charge supercurrent, it is necessary to integrate the current density along y over the junction width W . Since we assume that our system is translationally invariant along the y direction, the current density must of course also be y -independent. It is convenient then in the results that follow, to normalize the supercurrent, $I(x)$, by $I_0 \equiv WJ_0$. Having now outlined our general method and numerical approach, we proceed to present our numerical results and study the supercurrent for particular cases of SF and SF Josephson junctions.

III. RESULTS

In presenting our numerical results, we decompose the general charge supercurrent density [Eq. (23)] into each of its four components. The associated supercurrent subsequently has the components,

$$I_{S0}(x) = I_0 \int_{-\infty}^{\infty} d\varepsilon \{ \mathbb{S}(\varepsilon)\partial_x\mathbb{S}^*(-\varepsilon) - \mathbb{S}(-\varepsilon)\partial_x\mathbb{S}^*(\varepsilon) + \mathbb{S}^*(\varepsilon)\partial_x\mathbb{S}(-\varepsilon) - \mathbb{S}^*(-\varepsilon)\partial_x\mathbb{S}(\varepsilon) \} \tanh(\varepsilon\beta/2), \quad (24)$$

$$I_{Sx}(x) = I_0 \int_{-\infty}^{\infty} d\varepsilon \{ -\partial_x\mathbb{T}_x(-\varepsilon)\mathbb{T}_x^*(\varepsilon) + \partial_x\mathbb{T}_x(\varepsilon)\mathbb{T}_x^*(-\varepsilon) - \partial_x\mathbb{T}_x^*(-\varepsilon)\mathbb{T}_x(\varepsilon) + \partial_x\mathbb{T}_x^*(\varepsilon)\mathbb{T}_x(-\varepsilon) \} \tanh(\varepsilon\beta/2), \quad (25)$$

$$I_{Sy}(x) = I_0 \int_{-\infty}^{\infty} d\varepsilon \{ -\partial_x\mathbb{T}_y(-\varepsilon)\mathbb{T}_y^*(\varepsilon) + \partial_x\mathbb{T}_y(\varepsilon)\mathbb{T}_y^*(-\varepsilon) - \partial_x\mathbb{T}_y^*(-\varepsilon)\mathbb{T}_y(\varepsilon) + \partial_x\mathbb{T}_y^*(\varepsilon)\mathbb{T}_y(-\varepsilon) \} \tanh(\varepsilon\beta/2), \quad (26)$$

$$I_{Sz}(x) = I_0 \int_{-\infty}^{\infty} d\varepsilon \{ \partial_x\mathbb{T}_z(-\varepsilon)\mathbb{T}_z^*(\varepsilon) + \partial_x\mathbb{T}_z(\varepsilon)\mathbb{T}_z^*(-\varepsilon) - \partial_x\mathbb{T}_z^*(-\varepsilon)\mathbb{T}_z(\varepsilon) + \partial_x\mathbb{T}_z^*(\varepsilon)\mathbb{T}_z(-\varepsilon) \} \tanh(\varepsilon\beta/2). \quad (27)$$

The total charge current, $I_{tot}(x)$, is thus the sum,

$$I_{tot}(x) = I_{S0}(x) + I_{Sx}(x) + I_{Sy}(x) + I_{Sz}(x), \quad (28)$$

where I_{S0} denotes the singlet supercurrent component. We take the axis of spin quantization to lie along the z direction throughout the whole system, and thus the components I_{Sx} , I_{Sy} , represent the equal-spin triplet components with total spin projection of $m = \pm 1$ on the axis of spin quantization, while I_{Sz} , corresponds to opposite spin triplets with $m = 0$, and a total spin projection of zero.^{1,11,29,58,63} The decomposition of the supercurrent into the singlet and triplet components

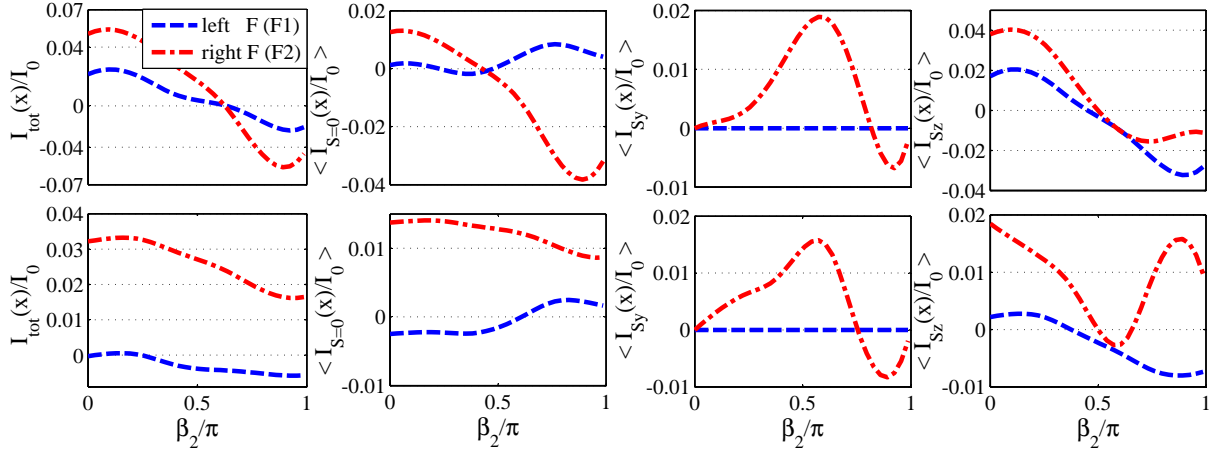


FIG. 2. (Color online) Total critical supercurrent (I_{tot}), singlet (I_{S0}), and odd-frequency (I_{Sy} , I_{Sz}) components of the Josephson $SF/SF/S$ structure. The current and the average of its components are shown as a function of exchange field orientation, β_2 (see Fig. 1). The averages are taken over the labeled magnetic regions. In the top row we assume $d_{F1} = d_{F2} = 0.4\xi_S$, and $d_S = 0.2\xi_S$. While in the bottom row $d_{F1} = 0.4\xi_S$, $d_{F2} = 0.7\xi_S$, and the thickness of middle superconducting lead is kept unchanged. We set the superconducting phase of the left, and middle superconductors to be $\theta_L = \theta_M = 0$ and $\theta_R = \pi/2$ (corresponding to the maximum supercurrent in this case, see text), respectively.

can also serve to identify the long range contributions to the supercurrent.^{29,30,58,63}

To begin, we first consider the simpler $SF/SF/S$ junction (Fig. 1, part *i*). We assume the far left SF interface is located at $x = 0$ and all interfaces reside in the yz plane. The thickness of F_1 , F_2 , and the middle superconducting lead are denoted by d_{F1} , d_{F2} , and d_S , respectively. Our theoretical framework permits each F layer to possess a general exchange field with arbitrary orientation, $\vec{h}_{1,2} = h_0(\cos \gamma_{1,2} \sin \beta_{1,2}, \sin \gamma_{1,2} \sin \beta_{1,2}, \cos \beta_{1,2})$. To study concrete examples, we consider systems with in-plane magnetization orientations where $\gamma_{1,2} = 0$, and thus rotation occurs in the yz plane. This also implies that β_1 and β_2 fully characterize the magnetization orientations of F_1 and F_2 , respectively, as illustrated in Fig. 1. The magnetization orientation of F_1 is assumed fixed in the z direction ($\beta_1 = 0$), while the magnetization in F_2 rotates with angle β_2 . We assume that the proximity effects related to the flow of spin-polarized supercurrent into the ferromagnetic regions has a negligible effect on their respective magnetizations.²¹ This assumption is frequently used in most of the theoretical works on the ferromagnetic multilayer Josephson configurations.^{10,11} As mentioned above, we also assume the macroscopic phases of the three superconducting leads (left, middle, and right), θ_L , θ_M , θ_R , are controlled externally.²¹ Throughout our calculations, we consider a low temperature of $T = 0.05T_c$, and a ferromagnetic strength given by the exchange field magnitude $|\vec{h}_{1,2}| = h_0 = 10\Delta_0$. Here T_c is the superconducting critical temperature and Δ_0 is the superconducting gap at zero temperature, also we set $k_B = \hbar = 1$. In this paper, all energies are normalized by Δ_0 while lengths are normalized by ξ_S , the superconducting coherence length. Since we have considered the low proximity tunneling limit in the diffusive regime, the interface transparencies affect the strength of the leakage of superconducting proximity correlations. In our actual calcu-

lations we have set $\zeta = 4$ which is consistent with the low proximity limit.

We first discuss the current phase relations, which are important for determining the experimentally relevant critical current, and the fundamental nature of resistanceless transport through junctions. When permissible, exact analytical current phase relationships can reveal more about the fundamental physics involved, and the important role of phase-coherent transport in Josephson junctions for practical device development. Also, since we have considered the low proximity limit in the diffusive regime, higher order harmonics are washed out.¹⁰ As mentioned in passing, exact analytical expressions are generally impossible in the types of systems considered here due to the complicated complex partial differential equations involved. Nonetheless, we were still able to extract simple current-phase relations from the full numerical results. We found that if the thickness of the middle superconductor is sufficiently thin, the coupling between the two outer superconductors results in supercurrent flow in the magnetic regions that obeys sinusoidal current-phase relations involving combinations of the three superconducting phases. Our numerical investigations have found that for our regimes of interest, the current phase relation in F_1 region obeys;

$$I_L = I_1 \sin \varphi_{LR} + I_2 \sin \varphi_{LM} + I_3 \sin \varphi_{RM} \sin \varphi_{LM}, \quad (29)$$

where $\varphi_{LR} = \theta_L - \theta_R$, $\varphi_{LM} = \theta_L - \theta_M$, and $\varphi_{RM} = \theta_R - \theta_M$. Here $I_{1,2,3}$ are constants which in general depend on geometry (d_{F1} , d_{F2} , d_S), temperature T , exchange fields $\vec{h}_{1,2}$, and interface transparencies ζ . In determining the current-phase relation above, several systematic investigations were numerically performed involving the macroscopic phases in each of the three terminals. Of the three phases, θ_R , θ_L , and θ_M , the supercurrent is calculated by varying one phase, e.g., θ_R , while the other two are kept fixed. This process is repeated for several differing fixed phases (say, θ_L and

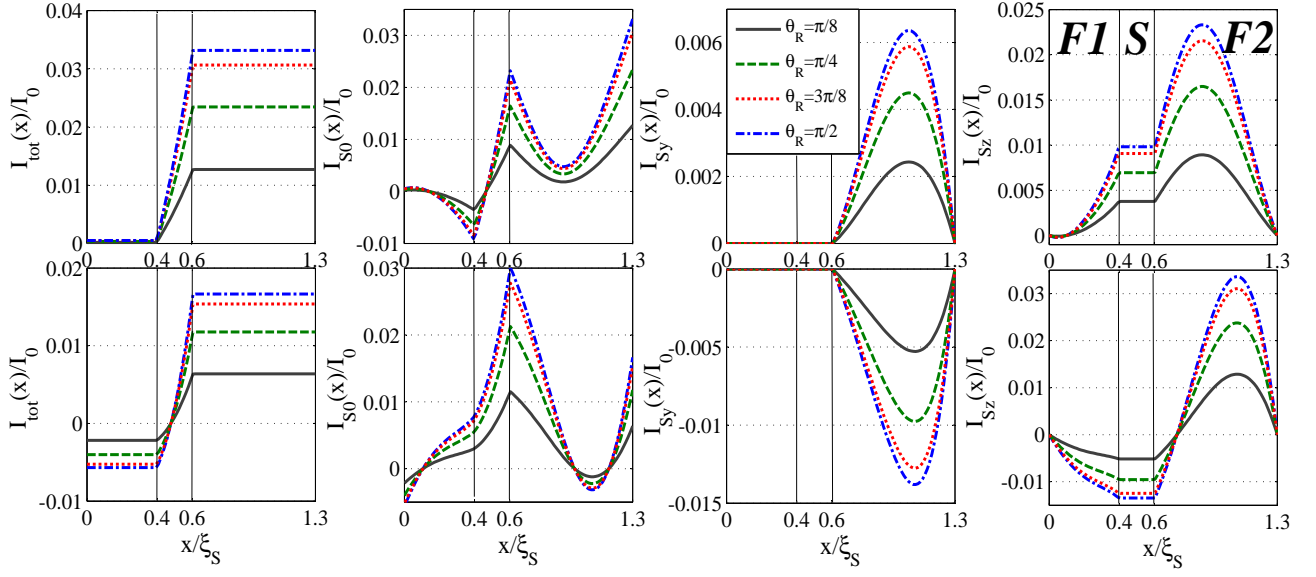


FIG. 3. (Color online) The Josephson current and its components (singlet (I_{S0}) and odd-frequency triplet ($I_{S_{y,z}}$)) vs position in an SF_1SF_2S junction for four values of the superconducting phase in the right terminal: $\theta_R = \pi/8, \pi/4, 3\pi/8, \pi/2$. We set $d_{F1} = 0.4\xi_S$, $d_{F2} = 0.7\xi_S$, $d_S = 0.2\xi_S$, and $\theta_L = \theta_M = 0$. The top row represents results where $\beta_2 = \pi/8$ while the bottom row shows results for $\beta_2 = 7\pi/8$. Throughout the paper we assume the exchange field direction in F_1 is oriented in the z direction, so that $\beta_1 = 0$. Different magnetic and superconducting regions are separated by vertical lines and marked by F_1 , F_2 , and S .

θ_M). This procedure also reveals the precise form of the coefficients $I_{1,2,3}$, which generally vary as the system parameters change. Below we present concrete examples that illustrate the relevant terms in the current-phase relation of Eq. (29). Unless otherwise noted, we set $\theta_L = \theta_M = 0$ and numerically vary θ_R . The precise nature of supercurrent transport in our three-terminal spin switch hinges crucially on not only the phase of the central S layer, but also its width. The geometrical effects of the central S layer can be seen in the limit of large d_S ($d_S \gg \xi_S$) where we find $I_L = 0$. This can be understood by noting that since $\varphi_{LM} = 0$, we have $I_L = I_1 \sin \varphi_{LR}$. Consequently for large d_S , the tunneling of quasiparticles through the middle S region is highly suppressed, giving $I_1 = 0 \Rightarrow I_L = 0$. For middle layers that are moderately thick (on the order of a few ξ_S), the last term in Eq. (29) implies (for $\varphi_{LM}, \varphi_{RM} \neq 0$) the two outer superconducting terminals are not entirely isolated from one another however. The effects of this coupling-term will be discussed in more detail below. Although we consider three superconducting terminals in serial, our findings are consistent with Ref. 64 where a cross diffusive ferromagnetic four-terminal Josephson transistor is studied. We have found that the sinusoidal relations are generally valid for the supercurrent when the relative magnetizations of the F layers are non-collinear. The relations (Eq. (29)) can thus be considered guides in determining phase differences that lead to optimal current flow. One such possibility involves the choice of $\theta_R = \pi/2$, which according to the sinusoidal relations, corresponds to maximum supercurrent flow, or equivalently the critical current, for the case when $\theta_L = \theta_M = 0$, and where the middle S is sufficiently thin ($I_1 \neq 0$, see Fig. 2). In other words, the critical current in a moderately thin middle S electrode and fixed

$\theta_L = \theta_M = 0$ occurs at $\theta_R = \pi/2$. We discuss below the benefits of situations where $\theta_L \neq \theta_M$.

Figure 2 exhibits the total Josephson current and its spatially averaged components through both ferromagnetic regions of the SF_1SF_2S system (Fig. 1 *i*), versus magnetization orientation of F_2 layer. We assume the magnetization orientation of F_1 is fixed along the z axis (spin quantization axis) while the exchange field in F_2 makes an angle β_2 with the z axis in the yz plane. This leads to vanishing \mathbb{T}_x , and \mathbb{T}_y components of the Green's function in F_1 . As discussed earlier, the macroscopic phase of the left and middle superconducting leads are $\theta_L = \theta_M = 0$ while $\theta_R = \pi/2$. The top row of the figure corresponds to equal-thickness magnets, with $d_{F1} = d_{F2} = 0.4\xi_S$, whereas the bottom row is for the same parameter set except now $d_{F1} = 0.4\xi_S$ and $d_{F2} = 0.7\xi_S$. As can be seen, the total current in both F_1 and F_2 depends on the magnetization rotation of F_2 . In the top row, the supercurrent in both F_1 and F_2 behave similarly. The current is positive when the relative magnetizations are in the parallel state ($\beta_2 = 0$), and then the current changes direction in the F_1 layer after $\beta_2 = \pi/2$, corresponding to perpendicular relative magnetization directions, and transition to a π state. Turning now to the individual components of the supercurrent, we see from the top panel of Fig. 2 that the singlet contribution, I_{S0} , follows some similar trends as the total current, but with different magnitudes. The average behavior of I_{S0} over the F regions are shown to both vanish at the same β_2 , indicating that the singlet part of the total supercurrent changes sign within the magnets. The possible spin-polarization effects due to the magnetization misalignment of the two F layers is revealed in the odd-frequency triplet con-

tributions, I_{Sy} , and I_{Sz} . The plots clearly demonstrate that the spin-1 projection of the triplet current, I_{Sy} , peaks in F_2 when the relative magnetizations are nearly orthogonal ($\beta_2 \approx \pi/2$), corresponding to nearly complete magnetization alignment along y . The I_{Sy} component meanwhile vanishes in F_1 as expected since the magnetization is aligned with the z quantization axis. The odd-frequency component, I_{Sz} , is typically finite in both magnets, possessing its largest value when their relative magnetizations are aligned along z . There is no average current flow when the relative magnetizations are approximately orthogonal ($\beta_2 = \pi/2$). Therefore, the device may also be viewed as a charge supercurrent switch controlled by magnetization orientation.

The bottom set of panels demonstrate that for differing F layer thicknesses the magnetization rotation can render one part of the system to be in a 0-state and the other to be in the π state. This suggests a 0- π spin switch that can arise by simply rotating the magnetization orientation in one of the ferromagnetic layers. Since $h_x = h_y = 0$ in F_1 , we have the \mathbb{T}_x and \mathbb{T}_y contributions to the supercurrent vanishing (see Eq. (23)). This is consequently also observed in the averaged equal-spin triplet current, $I_{Sy}(x)$. Note that we do not consider magnetizations out of plane, and therefore $I_{Sx}(x)$ necessarily vanishes throughout the system. To pinpoint the precise behavior of the total supercurrent and its spatially averaged triplet components, it is insightful to study their explicit spatial dependence.

In Fig. 3, we therefore illustrate the total charge supercurrent and its components as a function of position inside the three-terminal junction. Two representative angles $\beta_2 = \pi/8$ and $7\pi/8$ are chosen, and four different phases of the right superconductor, θ_R , are considered: $\pi/8$, $\pi/4$, $3\pi/8$, and $\pi/2$. The total current is piecewise constant in each non-superconducting region, reflecting local charge conservation. The central S region, however, acts as an external source of Cooper pairs, and thus the charge current in that region will acquire a position-dependence profile. This can be verified by considering the second set of panels from the left in Fig. 3, which depict the singlet contribution, $I_{S0}(x)$, as a function of position. The outer s -wave superconducting leads combined with the inhomogeneous magnetization provided by the two F layers, induces odd-frequency triplet correlations that naturally are location-dependent as well. This is observed in the other remaining panels. The middle S layer is void of any equal-spin, odd-frequency triplet correlations (I_{Sy}), but is populated with triplet I_{Sz} superconducting correlations that clearly depend on β_2 and θ_R . Examining the panels of Fig. 3, it is seen that the odd-frequency triplet component with nonzero spin projection, $I_{Sy}(x)$, vanishes in S . This is in contrast to the $I_{Sz}(x)$ contribution, which is constant inside the middle S terminal and equal to its value at the S/F interface. Thus within the middle S lead, the non-decaying odd-frequency triplet component, I_{Sz} , and the singlet component, I_{S0} , have a direct influence on supercurrent control. For this reason, within the F_1 region, the net supercurrent flow is seen to be due to the competition solely between I_{S0} and I_{Sz} (since I_{Sy} vanishes there), and which sometimes are oppositely directed. Magnetization rotation in F_2 can thus re-

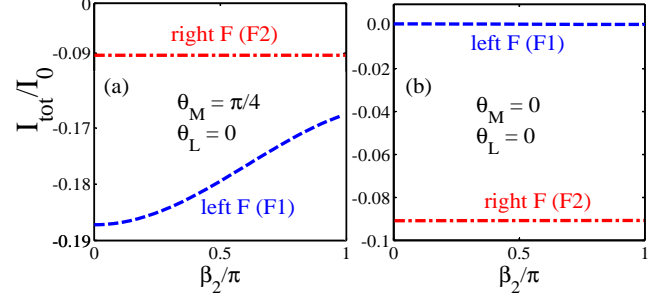


FIG. 4. (Color online) Total maximum supercurrent in each F region against β_2 , the magnetization orientation of F_2 in $SFSFS$ junction. Also, the magnetization in F_1 is fixed along the z axis, i.e., $\beta_1 = 0$. Here a thick middle S terminal is considered with $d_S = 4.0\xi_S$ corresponding to several tens of nanometers and $d_{F1} = 0.4\xi_S$, $d_{F2} = 0.7\xi_S$. (a) the macroscopic phase of the middle S terminal is fixed at $\theta_M = \pi/4$ while in (b) this quantity is set to zero, $\theta_M = 0$. In both cases, the macroscopic phase of the left superconducting terminal is $\theta_L = 0$ while θ_R varies in order to find the maximum supercurrent.

sult in total supercurrent flow there that is opposite to that of F_1 . Consequently the system resides in a composite 0- and π -state. Since the supercurrent is conserved inside the non-superconducting regions, this also implies that within the central S layer itself, the total supercurrent must undergo a reversal in direction.

As mentioned above, for large middle S layer widths, d_S , and $\theta_L - \theta_M = 0$, the outer S terminals should generally become decoupled, making it impossible to manipulate the current flowing in F_1 via magnetization rotation in F_2 . By externally tuning the macroscopic phase of the middle S layer however, the total maximum charge current in F_1 can now be controlled by the rotation of magnetization in F_2 . This is illustrated in Fig. 4, where the total current in each magnetic region of a $SFSFS$ structure is plotted versus the magnetization orientation of F_2 layer, β_2 . As before, the magnetization of F_1 is fixed along the z axis, i.e., $\beta_1 = 0$. The thicknesses of the F layers are $d_{F1} = 0.4\xi_S$, and $d_{F2} = 0.7\xi_S$, while a relatively thick middle S layer is set to $d_S = 4.0\xi_S$. This choice of d_S permits an analysis of the coupling and supercurrent roles of the middle S terminal. The superconducting phase of the left S terminal is fixed at $\theta_L = 0$, whereas θ_R varies over $[0, 2\pi]$ to determine the maximum supercurrent flow. In Fig. 4(a), the macroscopic phase of the middle S terminal is equal to $\theta_M = \pi/4$. As seen there, the supercurrent in F_2 is insensitive to magnetization direction, β_2 . This is consistent with the fact that charge supercurrent in a single SFS junction must be constant and independent of magnetization rotation. This is contrary to the supercurrent behavior in F_1 , where variations are shown as the magnetization vector rotates. In a way similar to what was observed in Fig. 3, the odd-frequency triplet current in F_2 is partially propagated through the middle S electrode into F_1 . The transport of these superconducting correlations into F_1 constitute a coupling mechanism between the outer S banks. Therefore, the odd-frequency triplet correlations and even-frequency singlet correlations together result

in changes to the supercurrent in F_1 by magnetization rotation of F_2 .

In Fig. 4(b) we further explore the proximity effects related to the width of the middle S terminal, where it now has a phase of zero ($\theta_M = 0$). It is evident that the total critical supercurrent in F_2 is non-zero and constant for all values of magnetization orientations, due to the nonzero phase difference between the middle and right S terminals. However, the supercurrent in F_1 vanishes despite a phase difference between the outer S terminals. This clearly demonstrates that for sufficiently thick middle S terminals and proper choice of phase differences, the outer S electrodes can become decoupled. We may summarize our results using Eq. (29) in the following way: For a supercurrent in F_1 and thick middle S layer, $d_S \gg \xi_S$, we have, $I_1 \rightarrow 0$. If we set then $\varphi_{LM} = 0$, no current flows through F_1 (see Fig. 4(b)). For the case of a thin middle S layer, and $\varphi_{LM} = 0$, the first term in Eq. (29) demonstrates that the magnitude of the supercurrent in F_1 is largest when $|\theta_L - \theta_R| = \pi/2$, in accordance with Fig. 2. When $\theta_R - \theta_M \neq 0$, and $\theta_L - \theta_M \neq 0$, the third term in Eq. (29) contributes to the generation of supercurrent (in addition to the non-zero second term). Interestingly, this coupling term involves the product of $\sin \varphi_{RM}$ and $\sin \varphi_{LM}$, which for our parameters, and S layers a few ξ_S thick, is the dominant term in Eq. (29). In this case, the coupling term reveals itself only in F_1 where there is a negative phase gradient, from right to left (see Fig. 4(a)). Thus, one may conclude that, e.g., if we set $\theta_L < \theta_M < \theta_R$, the middle S layer mediates supercurrent flow through F_1 via magnetization rotation in F_2 .

It is important to note that we have directly solved the Usadel equations (Eqs. (8)) in the F regions and the middle S electrode together with appropriate boundary conditions Eqs. (12) and (18). This way, we match the Green's function at the interfaces and thus the interaction of adjacent F regions for relatively thin middle S electrodes can be fully accounted for. If on the other hand, one uses the bulk solution given by Eq. (6) for the middle S electrode instead of solving the appro-

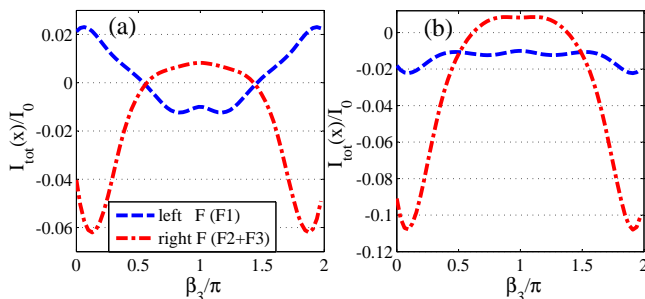


FIG. 5. (Color online) (a) Supercurrent in a $SFSSF$ junction where $\beta_1 = 0$, $\beta_2 = \pi$, and β_3 is varied. The geometrical parameters correspond to $d_S = 0.2\xi_S$, $d_{F1} = 0.4\xi_S$, and $d_{F2} = d_{F3} = 0.3\xi_S$. (b) Josephson current in the same structure with the same magnetization orientation, but now with $d_{F2} = 0.45\xi_S$, $d_{F3} = 0.15\xi_S$, and unchanged d_S . As done previously, we set $\theta_L = \theta_M = 0$ and $\theta_R = \pi/2$. The supercurrent is conserved within each magnetic layer (see Figs. 1 and 3). Thus the current is the same in the double ferromagnet regions as clearly seen in Fig. 6.

appropriate equations, the middle S region prohibits any transport between the adjacent F regions similar to the $d_S \gg \xi_S$ regime discussed earlier.

We now introduce additional magnetic inhomogeneity into the system by considering a more complicated $SFSSF$ structure as shown in part *ii*) of Fig. 1. The maximum value of the total charge current is shown in Fig. 5 over two regions: The F_1 region, and the F_2/F_3 double layer. Here the geometrical parameters correspond to $d_{F2} = d_{F3} = 0.3\xi_S$ (panel (a)) and $d_{F2} = 0.45\xi_S$, $d_{F3} = 0.15\xi_S$ (panel (b)). In both cases, $d_{F1} = 0.4\xi_S$, and $d_S = 0.2\xi_S$ (this value of d_S is correspond to the thin middle S electrode discussed earlier). We also set the phases, $\theta_L = \theta_M = 0$, and $\theta_R = \pi/2$. We vary the magnetization of the F_3 layer, β_3 , while fixing $\beta_1 = 0$, and $\beta_2 = \pi$. Thus the magnetization in F_1 is oriented along z , antiparallel to F_2 . As can be seen, the supercurrent direction and magnitude in each F region can be controlled by the magnetization orientation in F_3 . In panel (a) the total current in each ferromagnet is directed oppositely over the whole angular range of β_3 , except for $\beta_3 \approx \pi/2$ corresponding to magnetizations nearly orthogonal to the other two. In this case, there is a vanishing of the supercurrent in all F regions. The reversal of supercurrent direction in the F segments upon varying the magnetization orientation in the F_3 region, is in stark contrast to the findings of the previous $SFSSF$ case (bottom row of Fig. 2), where similar geometrical parameters were used. There the supercurrent changes direction in F_1 whereas it remains unchanged in F_2 by varying β_2 for the $d_{F1} = 0.4\xi_S$, and $d_{F2} = 0.7\xi_S$ case (where $d_{F2} > d_{F1}$). However, for the $SFSSF$ junction with equal F_2 , F_3 thicknesses (with $d_{F2} + d_{F3} > d_{F1}$), and parameters given in Fig. 5(a), we find the system has the 0 and π states coexisting over nearly the whole angular range of β_3 . An exception occurs near $\beta_3 \approx \pi/2$ and $3\pi/2$, where the supercurrent vanishes. It is also seen in Fig. 5 that the 0- and π -states exchange locations upon varying the magnetization rotation β_3 . In other words, the coexistence of 0- and π -states in the $SFSSF$ junction is now enhanced in the $SFSSF$ case. This interesting effect in $SFSSF$ junctions tends to wash out when $d_{F2} \neq d_{F3}$ (see Fig. 5(b)). It is apparent that the transport characteristics of $SFSSF$ Josephson junctions can be highly sensitive to the geometrical parameters and magnetization patterns. Clearly, the addition of the F_3 layer increases the possible tunable parameters, e.g., its width and magnetization orientation, so that more possibilities arise for spin switching and supercurrent control.

The behavior of the supercurrent as a function of magnetization variation in F_3 (Fig. 5) is consistent with the local spatial profile of the total supercurrent and its even and odd frequency components, exhibited in Fig. 6. In particular, the top panels illustrate that the total supercurrent is positive in throughout the F_1 region and then as β_3 increases, the current switches direction, becoming negative. The reverse trends are observed in the remaining ferromagnet regions, F_2 and F_3 , in accordance with Fig. 5(a). The valve effect is clearly identified for the perpendicular magnetic configuration (β_3), where the supercurrent nearly vanishes throughout the entire system. Turning now to the individual components of the total super-

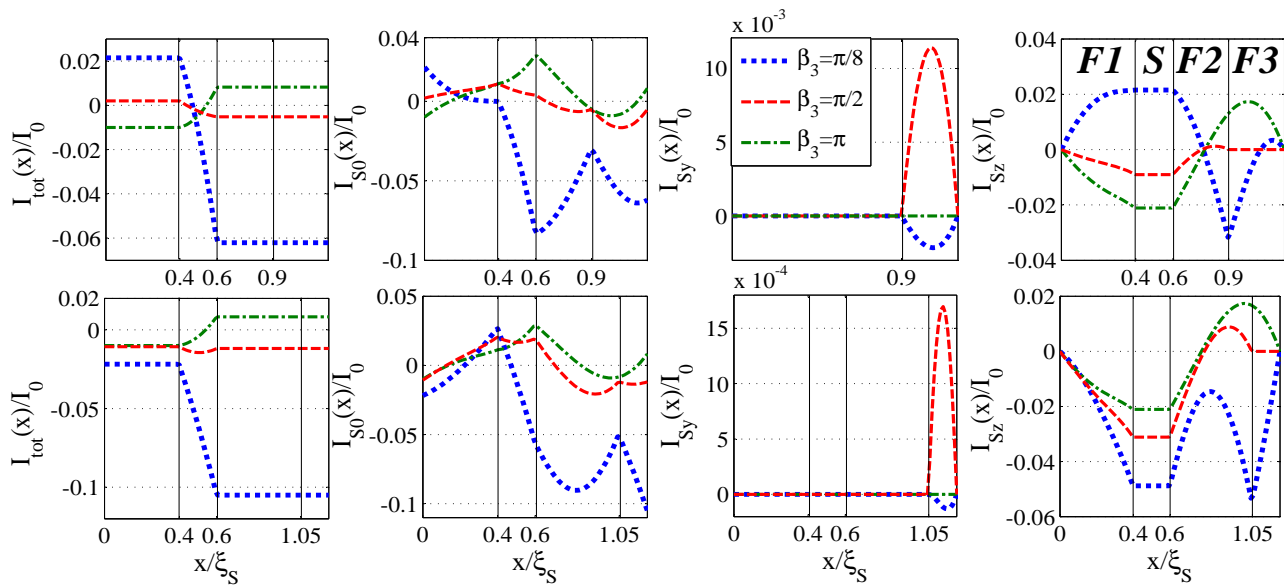


FIG. 6. (Color online) *SFSFS* junction (see Fig. 1). The spatial profiles of the Josephson supercurrent and its components (singlet (I_{S0}) and odd-frequency triplet ($I_{Sy,z}$)). The two magnetizations in F_1 and F_2 are fixed in an antiparallel configuration ($\beta_1 = 0, \beta_2 = \pi$) and three different magnetic orientations, β_3 , are considered for F_3 . The macroscopic phases, as before, are set to $\theta_L = \theta_M = 0$ and $\theta_R = \pi/2$. In all cases, the width of F_1 and middle S electrode are fixed at $d_{F1} = 0.4\xi_S$ and $d_S = 0.2\xi_S$, respectively. The other geometrical parameters correspond to (a) top row: $d_{F2} = d_{F3} = 0.3\xi_S$, and (b) bottom row: $d_{F2} = 0.45\xi_S, d_{F3} = 0.15\xi_S$. The vertical lines identify the interfaces of the junction among the magnetic and superconducting regions labeled by F_1, F_2, F_3 and S , respectively.

current, we see that although the current must be uniform in the F regions, the even and odd frequency contributions can have complicated spatial behavior. The spin-1 triplet component, I_{Sy} , is shown to vanish when all three magnetizations are collinear, which occurs when $\beta_3 = \pi$. As expected, it vanishes in the F_1 and F_2 regions for all β_3 since the relative magnetization there is always collinear. When the ferromagnet layers have magnetizations that are no longer collinear, spin-1 triplet correlations can be generated, which is largest in F_3 for $\beta_3 = \pi/2$.³² On the other hand, the triplet component, $|I_{Sz}|$ is largest when the magnetization angle corresponds to values closer to the z spin quantization axis, which in this case are $\beta_3 = \pi/8$ and π . Although similar trends are observed when considering unequal F widths (bottom row), the configuration involving larger d_{F2} and e.g., $\beta_3 = \pi/8$ permits I_{Sz} to establish a maximum in F_2 and subsequent decline towards the middle S , so that there is a greater contribution to negative total current flow compared to the symmetric case in the row above.

IV. CONCLUSIONS

In conclusion, we have considered *SFSFS* and *SFSFFS* systems which have been recently realized experimentally and are expected to have potential applications in the next generation of memories and quantum computers.^{2-4,6,17-21,65-67} We have considered the broadly accessible diffusive regime, which is applicable to many experimental conditions. Using the Keldysh-Usadel quasiclassical method, we demonstrated that in *SFSFS* and *SFSFFS* systems the behavior of the

supercurrent in a given *SFS* segment can remarkably be controlled simply by the magnetization orientation in the other ferromagnetic regions. We have shown that $0-\pi$ state profiles of each junction segment is controllable by means of magnetization rotation. Particularly, the magnetization rotation can render one part of the junction to be in a 0 state while the other can be in a π state. In other words, the system can be in both a 0 and π state configuration: a three-terminal $0-\pi$ spin switch. We have investigated the current-phase relations in such structures numerically, and formulated our findings. Our results revealed that a relatively thick middle S electrode can act as an external source of supercurrent or can effectively limit the spin-tuned transport through the system, depending on the macroscopic superconducting phases. We have analyzed the origin of such aspects by decomposing the total supercurrent into its even-frequency singlet and odd-frequency triplet components. We have shown that the triplet correlations propagate through the middle superconductor terminal without any decline in their amplitude. This is suggestive of a superconducting spin-switch with controllable charge supercurrent using the magnetization rotation of a ferromagnetic layer constituting the *SFSFS* and *SFSFFS* systems.

ACKNOWLEDGMENTS

M.A. would like to thank G. Sewell for valuable discussions in numerical parts of this work. K.H. is supported in part by ONR and by a grant of supercomputer resources provided by the DOD HPCMP.

V. PAULI MATRICES

In Sec. II we introduced the the 2×2 Pauli matrices in spin space. They are denoted by $\vec{\tau} = (\tau_1, \tau_2, \tau_3)$, and given by,

$$\tau_1 = \begin{pmatrix} 0 & 1 \\ 1 & 0 \end{pmatrix}, \quad \tau_2 = \begin{pmatrix} 0 & -i \\ i & 0 \end{pmatrix}, \quad \tau_3 = \begin{pmatrix} 1 & 0 \\ 0 & -1 \end{pmatrix}.$$

We also introduced the 4×4 matrices $\vec{\hat{\rho}} = (\hat{\rho}_1, \hat{\rho}_2, \hat{\rho}_3)$:

$$\hat{\rho}_1 = \begin{pmatrix} 0 & \tau_1 \\ \tau_1 & 0 \end{pmatrix}, \quad \hat{\rho}_2 = \begin{pmatrix} 0 & -i\tau_1 \\ i\tau_1 & 0 \end{pmatrix}, \quad \hat{\rho}_3 = \begin{pmatrix} \tau_0 & 0 \\ 0 & -\tau_0 \end{pmatrix}.$$

To simplify expressions, it is also convenient to use the following definitions:

$$\tau_0 = \begin{pmatrix} 1 & 0 \\ 0 & 1 \end{pmatrix}, \quad \hat{\rho}_0 = \begin{pmatrix} \tau_0 & 0 \\ 0 & \tau_0 \end{pmatrix}.$$

-
- * phymalidoust@gmail.com
† klaus.halterman@navy.mil
- ¹ K.B. Efetov, I.A.Garifullin, A.F.Volkov, K.Westerholt, *Magnetic Heterostructures. Advances and Perspectives in Spinstructures and Spintransport*. ed. by H. Zabel, S.D. Bader, Series. Springer Tracts in Modern Physics, vol 227 (Springer, New York, 2007), P. 252
 - ² M. Eschrig, Phys. Today **64**, 43 (2011).
 - ³ F. Giazotto, J. T. Peltonen, M. Meschke, and J. P. Pekola, Nat. Phys. **6**, 254 (2010).
 - ⁴ F. Giazotto, P. Spathis, S. Roddaro, S. Biswas, F. Taddei, M. Governale, and L. Sorba, Nat. Phys. **7**, 857 (2011).
 - ⁵ P. Spathis, S. Biswas, S. Roddaro, L. Sorba, F. Giazotto, and F. Beltram, Nanotechnology **22**, 105201 (2011).
 - ⁶ M. Alidoust, K. Halterman, and J. Linder, Phys. Rev. B **88**, 075435 (2013).
 - ⁷ E.A. Demler, G.B. Arnold, and M.R. Beasley, Phys. Rev. B **55**, 15174 (1997).
 - ⁸ K. Halterman and O.T. Valls, Phys. Rev. B **65**, 014509 (2001).
 - ⁹ A.A. Golubov, M.Yu. Kupriyanov, E. Il'ichev, Rev. Mod. Phys. **76**, 411 (2004).
 - ¹⁰ A. Buzdin, Rev. Mod. Phys. **77**, 935 (2005).
 - ¹¹ F.S. Bergeret, A.F. Volkov, K.B. Efetov, Rev. Mod. Phys. **77**, 1321 (2005).
 - ¹² V.V. Ryazanov, V.A. Oboznov, A.Yu. Rusanov, A.V. Vereten'nikov, A.A. Golubov, and J. Aarts, Phys. Rev. Lett. **86**, 2427 (2001).
 - ¹³ L.N. Bulaevskii, V.V. Kuzii, A.A. Sobyenin, JETP Lett. **25**, 290 (1977).
 - ¹⁴ A.I. Buzdin, L.N. Bulaevskii, S.V. Panyukov, JETP Lett. **35**, 178 (1982).
 - ¹⁵ Y. Makhlin, G. Schoen, A. Shnirman, Rev. Mod. Phys. **73**, 357 (2001).
 - ¹⁶ F.S. Bergeret, A.F. Volkov, K.B. Efetov, Phys. Rev. Lett. **86**, 4096 (2001).
 - ¹⁷ V.V. Ryazanov, V.V. Bolginov, D.S. Sobanin, I.V. Vernik, S.K. Tolpygo, A.M. Kadin, O.A. Mukhanov, Physics Procedia **36**, 35 (2012).
 - ¹⁸ I.T. Larkin, V.V. Bolginov, V.S. Stolyarov, V.V. Ryazanov, I.V. Vernik, S.K.T. and O.A. Mukhanov, Appl. Phys. Lett. **100**, 222601 (2012).
 - ¹⁹ S.V. Bakurskiy, N.V. Klenov, I.I. Soloviev, V.V. Bolginov, V.V. Ryazanov, I.V. Vernik, O.A. Mukhanov, M.Yu. Kupriyanov and A.A. Golubov, Appl. Phys. Lett. **102**, 192603 (2013).
 - ²⁰ I.V. Vernik, V.V. Bolginov, S.V. Bakurskiy, A.A. Golubov, M.Y. Kupriyanov, V.V. Ryazanov, and O.A. Mukhanov, IEEE Tran. Appl. Supercond. **23** 1701208 (2013).
 - ²¹ N. Pugach, and A. Buzdin, Appl. Phys. Lett. **101**, 242602 (2012).
 - ²² K. Halterman and O.T. Valls, Phys. Rev. B **69**, 014517 (2004).
 - ²³ S.V. Bakurskiy, N.V. Klenov, I.I. Soloviev, M.Yu. Kupriyanov, and A.A. Golubov Phys. Rev. B **88**, 144519 (2013).
 - ²⁴ J.W.A. Robinson, J.D.S. Witt, M.G. Blamire, Science **329**, 5987 (2010).
 - ²⁵ M. Alidoust, and J. Linder, Phys. Rev. B **82**, 224504 (2010).
 - ²⁶ G.B. Halasz, M.G. Blamire, and J.W.A. Robinson, Phys. Rev. B **84**, 024517 (2011).
 - ²⁷ C. Wu, O.T. Valls, and K. Halterman, Phys. Rev. Lett. **108**, 117005 (2012).
 - ²⁸ M. Alidoust, J. Linder, G. Rashedi, T. Yokoyama, and A. Sodbo, Phys. Rev. B **81**, 014512 (2010).
 - ²⁹ I.B. Sperstad, J. Linder, and A. Sudbø, Phys. Rev. B **78**, 104509 (2008).
 - ³⁰ M. Alidoust, K. Halterman, and J. Linder, Phys. Rev. B **89**, 054508 (2014).
 - ³¹ A.G. Malshukov, and A. Brataas, Phys. Rev. B **86**, 094517 (2012).
 - ³² M. Houzet, A. I. Buzdin, Phys. Rev. B **74**, 214507 (2006).
 - ³³ C. Richard, M. Houzet, J. S. Meyer, Phys. Rev. Lett. **110**, 217004 (2013).
 - ³⁴ A. Cottet, T. Kontos, W. Belzig, C. Schonenberger, C. Bruder, Europhys. Lett. **74**, 320 (2006).
 - ³⁵ A.V. Zaitsev, Zh. Eksp. Teor. Fiz. **86**, 1742 (1984) (Sov. Phys. JETP **59**, 1015 (1984); M.Y. Kupriyanov *et al.*, Sov. Phys. JETP **67**, 1163 (1988).
 - ³⁶ Z. Pajovic, M. Bozovic, Z. Radovic, J. Cayssol, and A. Buzdin, Phys. Rev. B **74**, 184509 (2006).
 - ³⁷ Y.S. Barash, I.V. Bobkova, and T. Kopp, Phys. Rev. B **66**, 140503(R) (2002).
 - ³⁸ B. Crouzy, S. Tollis, and D.A. Ivanov, Phys. Rev. B **76**, 134502 (2007).
 - ³⁹ H. Sellier, C. Baraduc, F. Lefloch, and R. Calemczuk, Phys. Rev. Lett. **92**, 257005 (2004).
 - ⁴⁰ Ya.V. Fominov, A.F. Volkov, and K.B. Efetov, Phys. Rev. B **75**, 104509 (2007).
 - ⁴¹ Y. Asano, Y. Sawa, Y. Tanaka, and A.A. Golubov, Phys. Rev. B **76**, 224525 (2007).
 - ⁴² Y. Asano, Y. Tanaka, T. Yokoyama, and S. Kashiwaya, Phys. Rev. B **74**, 064507 (2006).
 - ⁴³ G. Eilenberger, Z. Phys. **214**, 195 (1968).
 - ⁴⁴ K. Usadel, Phys. Rev. Lett. **25**, 507 (1970).
 - ⁴⁵ I. Sosnin, H. Cho, V. T. Petrashov, and A.F. Volkov, Phys. Rev. Lett. **96**, 157002 (2006).
 - ⁴⁶ N.G. Pugach, M.Yu. Kupriyanov, A.V. Vedyayev, C. Lacroix, E. Goldobin, D. Koelle, R. Kleiner, and A.S. Sidorenko Phys. Rev. B **80**, 134516 (2009).
 - ⁴⁷ G.B. Halsz, J.W. A. Robinson, J.F. Annett, and M.G. Blamire, Phys. Rev. B **79**, 224505 (2009).

- ⁴⁸ T. Kontos, M. Aprili, J. Lesueur, X. Grison, Phys. Rev. Lett. **86**, 304 (2001).
- ⁴⁹ R.S. Keizer, S.T. B. Goennenwein, T.M. Klapwijk, G. Miao, G. Xiao and A. Gupta, Nature **439**, 825 (2006).
- ⁵⁰ M. Eschrig, T. Lofwander, Nat. Phys. **4**, 138 (2008).
- ⁵¹ T.S. Khaire, M.A. Khasawneh, W.P. Pratt, N.O. Birge, Phys. Rev. Lett. **104**, 137002 (2010).
- ⁵² T. Lofwander, T. Champel, J. Durst, M. Eschrig, Phys. Rev. Lett. **95**, 187003 (2005).
- ⁵³ S. Hikino and S. Yunoki, Phys. Rev. Lett. **110**, 237003 (2013).
- ⁵⁴ A.M. Bobkov and I.V. Bobkova, Phys. Rev. B **84**, 054533 (2011); Phys. Rev. Lett. **108**, 197002 (2012).
- ⁵⁵ L. Trifunovic, Z. Popovic, and Z. Radovic, Phys. Rev. B **84**, 064511 (2011).
- ⁵⁶ L. Trifunovic, Phys. Rev. Lett. **107**, 047001 (2011).
- ⁵⁷ L.J. Jin, Y. Wang, L. Wen, G.Q. Zha, and S.P. Zhou Physics Letters A **376**, 2435 (2012).
- ⁵⁸ M. Eschrig, J. Kopu, J.C. Cuevas, and G. Schon, Phys. Rev. Lett. **90**, 137003 (2003).
- ⁵⁹ K. Halterman, P. H. Barsic, and O.T. Valls, Phys. Rev. Lett. **99**, 127002 (2007).
- ⁶⁰ K. Halterman and O. T. Valls, Phys. Rev. B **80**, 104502 (2009).
- ⁶¹ V. Braude and Yu.V. Nazarov, Phys. Rev. Lett. **98**, 077003 (2007).
- ⁶² J.P. Morten, M.S. thesis, Norwegian University of Science and Technology, 2003.
- ⁶³ A.F. Volkov and K.B. Efetov, Phys. Rev. B **81**, 144522 (2010).
- ⁶⁴ M. Alidoust, G. Sewell, and J. Linder Phys. Rev. B **85**, 144520 (2012).
- ⁶⁵ L.B. Ioffe, V.B. Geshkenbein, M.V. Feigelman, A.L. Fauchere, and G. Blatter, Nature (London) **398**, 679 (1999).
- ⁶⁶ G. Binasch, P. Grunberg, F. Saurenbach, and W. Zinn, Phys. Rev. B **39**, 4828 (1989).
- ⁶⁷ M.N. Baibich, J.M. Broto, A. Fert, F. Nguyen Van Dau, F. Petroff, P. Eitenne, G. Creuzet, A. Friederich, and J. Chazelas, Phys. Rev. Lett. **61**, 2472 (1988).
- ⁶⁸ M. Vissers, V. K. Chua, S. A. Law, S. Vishveshwara, J. N. Eckstein, arXiv:1402.6055.
- ⁶⁹ J. D. Sau, R. M. Lutchyn, S. Tewari, S. D. Sarma Phys. Rev. Lett. **104**, 040502 (2010).
- ⁷⁰ R. M. Lutchyn, J. D. Sau, and S. D. Sarma. Phys. Rev. Lett. **105**, 077001 (2010).
- ⁷¹ J. Alicea, Y. Oreg, G. Refael, F. v. Oppen, M. P. A. Fisher, Nat. Phys. **7**, 412 (2011).
- ⁷² V. Mourik, K. Zuo, S.M. Frolov, S.R. Plissard, E.P.A.M. Bakkers, L.P. Kouwenhoven, Science, **336**, 1003 (2012).